Journal of Computer Science

Research Article

Auto Weight Dilated Convolutional Ensemble Network for the Severity Analysis of Lung Cancer in CT Images

L. Sandhya and K. Marimuthu

Department of Computer Science and Engineering, Presidency University, Bangalore, India

Article history
Received: 16-04-2025
Revised: 31-07-2025
Accepted: 04-09-2025

Corresponding Author:
L. Sandhya
Department of Computer Science and Engineering, Presidency University, Bangalore, India
Email: saisandhyalaxcse@gmail.com

Abstract: Lung cancer is one of the world's leading causes of morbidity and mortality; improving patient outcomes requires an early and precise diagnosis. Lesion and tumor segmentation remains a challenging task in CT images due to their inherent imaging limitations, such as the small size of nodules, heterogeneous textures, blurry boundaries, and adjacent structures, leading to misclassification and difficulty in delineating boundaries. To analyse the severity of lung cancer in CT images, the Auto Weight Dilated Convolutional Ensemble Network (AWDCE-Net) was developed in this article. To extract features of multi-scale lung pulmonary nodules, we created the AD-Net, or auto-weight dilated convolution network. In particular, multi-scale convolutional feature maps were employed by the Auto-weight Dilated convolutional (AD) unit to collect the MA features' auto-weight scales. Using a learnable set of parameters, the AD unit fused convolutional feature maps in encoding layers. The AD unit is a helpful design for feature extraction during the encoding process. We combined the advantages of the U-Net network for both shallow and deep features with the AD unit. AWDCE-Net's exceptional effectiveness in processing lung cancer CT images is demonstrated by experimental evaluation on the IQ-OTH/NCCD dataset, which yielded an accuracy of 99.12% and an F1-measure of 99.12%. With accuracy and F1-score improvements of 2.18 and 1.51%, respectively, these measurements show a significant improvement over popular models.

Keywords: Lung CT Image, Classification, Self-Refinement, Feature Fusion Module

Introduction

In scientific research, medical diagnosis, and treatment, medical imaging is essential. It gives physicians useful diagnostic information by displaying the patient's body structure and functions in an understandable manner. As medical imaging technology continues to advance (Lundervold and Lundervold, 2019), it has become an essential tool for disease diagnosis and the creation of individualized treatment regimens (Cheng et al., 2016). Additionally, inter-observer variability may have an adverse effect on the diagnostic consistency of manual examination. Artificial intelligence is used by Computer-Aided Diagnostic (CAD) systems to help increase efficiency in order to handle such issues. Because they can directly extract hierarchical features from the input data, convolutional neural networks in particular have shown excellent performance in picture classification. CNNs have been used more recently for tumor classification, segmentation, and detection. One of the primary benefits of these automated diagnostic systems is that they provide quicker interpretations, which lessens the workload for radiologists (Sluimer et al., 2006). Additionally, transfer learning has shown promise. By capturing global information and long-range relationships, transformer-based architectures and attention mechanisms have started to outperform conventional CNN techniques. Nevertheless, their implementation is computationally costly (Tharwat et al., 2022; Bade and Dela, 2020).

Medical image classification plays a foundational role in computer-aided diagnosis systems, enabling automated disease detection, subtype differentiation, and clinical decision support (Lundervold and Lundervold, 2019; Cheng et al., 2016; Tharwat et al., 2022; Bade and Dela, 2020; Bray et al., 2024; Siegel et al., 2022). It serves as a critical

component in early-stage screening, pathological stratification, and outcome prediction across a wide range of imaging modalities. Despite rapid advances driven by deep learning, developing models that remain accurate and robust under clinical conditions continues to pose significant challenges. Medical images often suffer from three key issues: Blurred or diffuse lesion boundaries that obscure precise localization, heterogeneous textures and background noise that reduce discriminative power, and variations in resolution and scale that hinder cross-dataset generalization.

Deep learning has brought significant breakthroughs in medical image classification, enabling more accurate and automated disease recognition across a wide spectrum of clinical scenarios such as colorectal cancer detection (Adams et al., 2023), gastrointestinal lesion diagnosis (Sluimer et al., 2006), and digital pathology analysis (Gould et al., 2013). Among the many architectures explored, Convolutional Neural Networks (CNNs) have long served as the cornerstone due to their strong inductive biases and hierarchical feature composition (Ciello et al., 2017). These properties make CNNs especially effective for capturing localized structures such as edges, textures, and gland boundaries, which are essential for recognizing most anatomical and pathological patterns. As a result, CNN-based models like ResNet (McDonald et al., 2015), DenseNet (Hanna et al., 2018), and EfficientNet (De Margerie-Mellon and Chassagnon, 2023) have been widely adopted in tasks such as tumor grading and polyp classification.

Lung cancer is one of the most common and deadly cancer diseases worldwide, with high morbidity and mortality rates. Research on Cancer's most recent projections indicate that lung cancer is expected to be the leading cancer type in 2022, with nearly 2.5 million new diagnoses, representing 12.4% of all global cancer cases (Bray et al., 2024). In its early stages, lung cancer often has no obvious symptoms, and many patients are not diagnosed until they develop late symptoms such as persistent cough, chest pain, dyspnea, or weight loss, resulting in a lower overall survival rate (Siegel et al., 2022). Pulmonary nodules are one of the early signs of lung cancer. Timely detection and monitoring of pulmonary nodules is very important for early identification of lung cancer. Imaging examinations can help detect nodules in the lungs, making early diagnosis possible, thereby significantly improving patient prognosis and survival rates (Adams et al., 2023).

Lesion and tumor segmentation remains a challenging task in CT images due to their shadowing and indistinct tissue boundaries. CT is widely used for lung cancer screening, allowing radiologists to assess the risk of lung cancer by identifying and segmenting lung nodules (Sluimer et al., 2006). First, segmenting lung nodules can extract the morphological features of nodules and provide a basis for judging whether the nodules are benign or malignant by determining whether the nodules have regular shapes and clear boundaries. Moreover, as shown in Fig. 1, various lung nodule types, such as solid, partially solid, and calcified, exhibit distinct morphologies and characteristics, highlighting the need for prompt and precise screening and diagnosis (Gould et al., 2013). However, identifying lung nodules on chest CT is a tedious and challenging task (Ciello et al., 2017). Each chest CT image may contain hundreds of slices, and radiologists must spend a lot of time and energy to examine each set of images (McDonald et al., 2015). As lung cancer screening advances, the number of chest CT scans is expected to rise, which could lead to an increase in diagnostic errors by radiologists due to the higher workload (Hanna et al., 2018; De Margerie-Mellon and Chassagnon, 2023).

A brief explanation of Lung cancer subtypes is given below:

- Adenocarcinoma: Making up to 40% of all cases, adenocarcinoma is the most common histologic subtype of non-small cell lung cancer (Adams et al., 2023). Squamous Cell Carcinoma usually appears in the central airway, such as the left or right bronchus, or the central lung (Sluimer et al., 2006)
- Large Cell Carcinoma: The third type of NSCLC, large cell carcinoma, affects the outer parts of the lungs. It only makes up about 10% of cases when compared to other forms of NSCLC (Gould et al., 2013)

The overall flow diagram of the Ensemble model for severity analysis of lung cancer is given in Figure 2.

Related Work

Early detection and treatment of lung cancer is critical to saving lives. When malignant cells in one or both lungs grow out of control, it can lead to lung cancer, a potentially fatal condition that can spread to other organs if left untreated. An efficient Computer-Aided Diagnostic (CAD) system that can more accurately identify and categorize lung cancer is therefore desperately needed. This section will provide a thorough discussion of the methodologies, tactics, techniques, and phases of lung image processing used by different authors in the literature to detect lung cancer.

Fully Convolutional Network (FCN) (Long et al., 2015) pioneered a pixel-wise prediction architecture for semantic segmentation. U-Net (Ronneberger et al., 2015) introduced an encoder for capturing context and a decoder that supports precise positioning, with the advantage of a simple and efficient architecture that only requires a few data points for training. Subsequently, the U-shaped architecture was improved and applied to image segmentation in various ways. UNet++ (Zhou et al., 2020) Designed a new skip connection based on dense connections for more flexible feature fusion. Attention U-

Net (Nitha et al., 2024) introduces the Attention Gate (AG) mechanism, which allows the model to focus on specific local regions and suppress the influence of irrelevant regions. Compared to the global attention mechanism, it is more suitable for dense small object segmentation.

ResUNet++ (Jha et al., 2019) introduced Atrous Spatial Pyramidal Pooling and attention modules into the network, allowing context information to be captured at different scales and focusing on important areas of the feature map. Meanwhile, the proposed attention mechanism enables the model to focus more precisely on characteristic regions of lung nodules, thereby achieving higher segmentation accuracy in complex backgrounds. Through these enhancements, the proposed model aims to provide a more effective solution for lung nodule segmentation tasks.

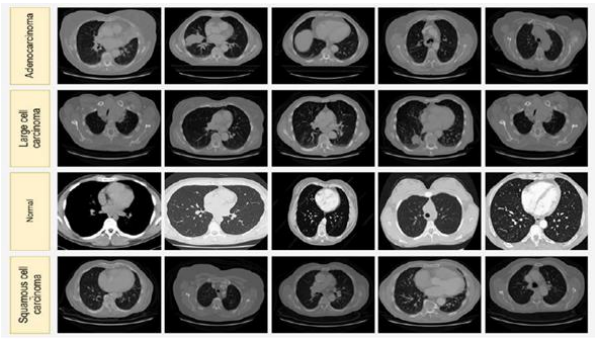

Fig. 1: Multi-class lung cancer CT images

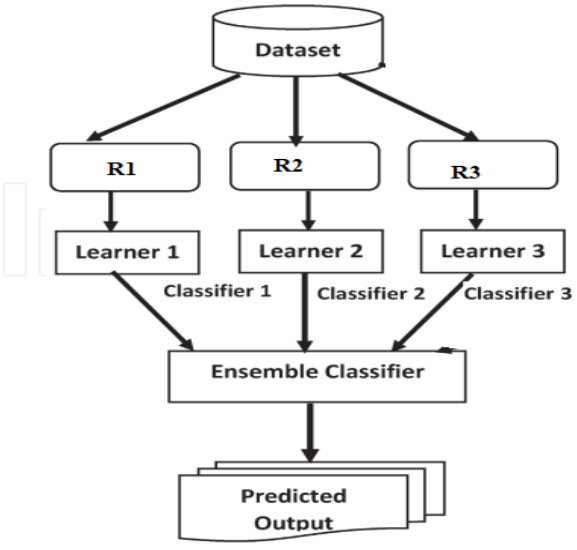

Fig. 2: Ensemble framework for prediction and classification of Lung cancer CT images

In this study, a deep learning-based model is proposed to solve the lung cancer classification problem. The model combines multi-level features using parallel feature learning, while the parallel operation of dilated and deformable convolution layers effectively extracts features with different scales and shape variations. Specifically, dilated convolutions capture more contextual information over an expanded area, while deformable convolutions use dynamic receptive fields to adapt to variations in the shape and size of objects. The parallel integration of these two techniques enhances the model's ability to detect both small and large lung nodules, thereby optimizing classification performance. The success of the model was tested on different datasets obtained from public lung cancer datasets, IQ-OTH/NCCD, and LIDC-IDRI. Using a variety of methods, these algorithms have demonstrated good accuracy and sensitivity rates. These investigations using a variety of AI and DL techniques have significantly improved the diagnosis of lung cancer and demonstrated encouraging outcomes in the areas of early detection and classification.

Auto Weight Dilated Convolutional Ensemble Model

Lung cancer has a high mortality rate and is a fatal disease. Computed Tomography (CT) image segmentation of the lung automatically is useful for the patient's subsequent diagnosis and therapy. The overall network structure framework is shown in Figure 1. The input image to be segmented is processed in the model for feature extraction. The Multi-Scale Feature Compensation Module (MFCM) integrates features between adjacent encoders. The features at different scales are extracted with pooling operations of different sizes and dilated convolutions of different expansion rates. The Subtraction Fusion Module (SFM) uses attention mechanisms to focus on target features in both channel and spatial dimensions. The feature differences are employed to help target localization, reduce feature redundancy, and enhance the robustness of the model. Additionally, a branch is introduced on the encoding path to extract the frequency domain features. The Wavelet Attention Enhancement Module (WAEM) is designed. The wavelet transform can better capture local changes and features. The wavelet transform extracts low-frequency information by decomposing the signal into different frequency sub-bands. The low-frequency information extracted by the wavelet transform focuses more on overall structures, while the features extracted by max-pooling focus more on local features. By concatenating the features from the two branches, the diversity of features is enriched.

Figure 3 shows the suggested design for a multiclass lung cancer classification system. The network is primarily composed of the linear up-sampling, the AD unit, the residual (Res) unit, the first and last convolution

units, and other components. During the down-sampling procedure (also called feature coding extraction), we generate multi-scale feature maps using 8 AD units. In the up-sampling stage (feature decoding), we combine the AD unit, the Res unit, and a linear up-sampling layer to create a primary decoding layer. After that, a convolution unit generates the output of the network model. For multiclass lung cancer classification, batch normalization and ReLU functions are also integrated into each convolution unit, AD unit, and Res unit.

We used two convolution units to reduce and then increase the number of convolution kernels in the Res Unit layer for the Res block shown in Figure 4(b), in order to accomplish feature learning and feature map reorganization.

We started with two convolution units (like the Res unit) for the AD Unit layer in Fig. 4(a). The network's feature extraction capabilities could be enhanced by utilizing the two kinds of convolutions. As shown in Fig. 5, we employed three neural networks (Block-R1, Block-R2, and Block-R3) and three alternative residual units in place of the AD unit in order to more precisely evaluate its performance. In the encoder step, every residual block is a dual-pathway structure. The current channel depth settings are 256, 128, 64, and 32. The residual block is the most important component in downsampling. In the decoder stage, we upsample by connecting a convolutional and a deconvolutional unit. The kernel size is 3×3×3, and the stripe of the deconvolutional unit is 2×2×2.

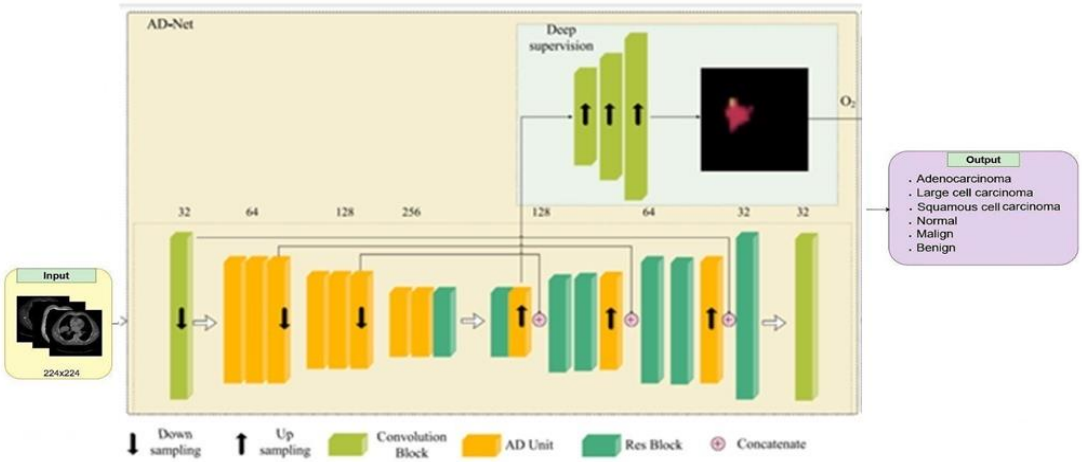

Fig. 3: An illustration of the proposed architecture for a multi-class lung cancer classification system

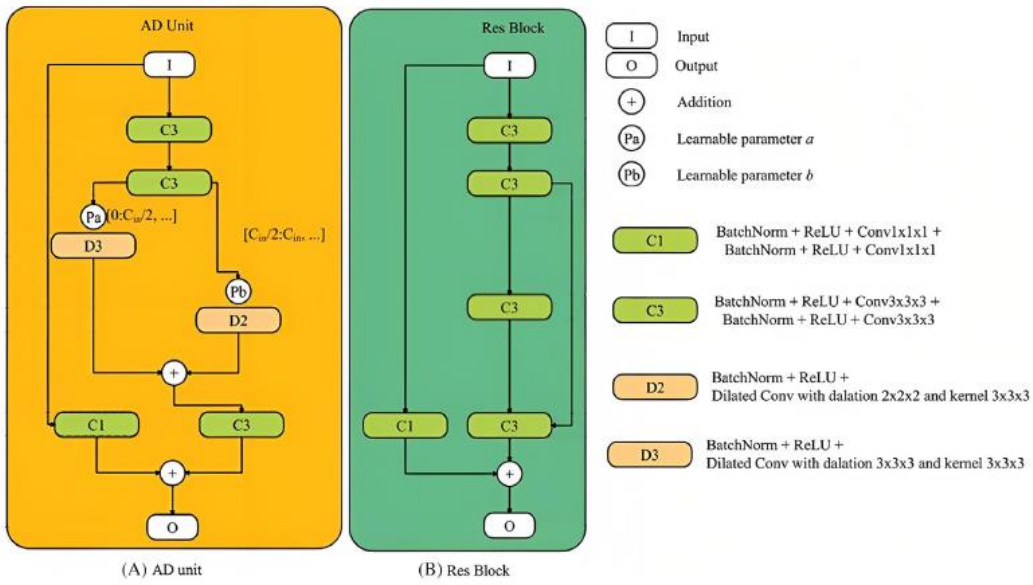

Fig. 4: Detailed architecture of the proposed Ensemble model (a) AD unit. (b) Res block unit

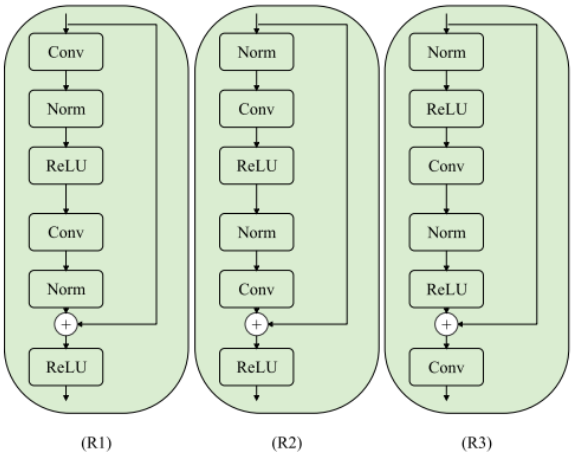

Fig. 5: The different residual convolution blocks

Every convolutional and deconvolutional unit in this step is connected to the convolutional or deconvolutional units by batch normalization and ReLU activation functions. Similarly, we set the channel depth of the decoder stage to 32×64×128×256. The remaining blocks allow a deep neural network to generate deeper layers with more pronounced gradients when combined with the network. As a result, gradient vanishing is a very uncommon phenomenon that benefits from MAs' more useful characteristics. The gradient propagation formula, which can be defined in the convolutional layer, is specified by Equation (1):

$$\delta_1 = \sigma^r(Out_l)\,(w_{l+1})^T \delta_{l+1} Out_l \tag{1}$$

Gradient in Block-R1, Block-R2 and Block-R3 can be defined as per Equation (2):

$$\begin{aligned} Out_{r^1_{l+1}} &= f(\delta_2(out_{r1_l})) + Out_{r1_l})) \\ Out_{r^2_{l+1}} &= f(\delta_2(f(\delta(out_{r2_l})) + Out_{r2_l})) \\ Out_{r^3_{l+1}} &= \delta_2(f(\delta_1(f(out_{r3_l})) + O_{utr3_l})) \end{aligned} \tag{2}$$

Where f means the activation function, δ_1 and δ_2 represent the first and second convolution calculations, respectively.

Results and Discussion

Data Sets and Evaluation Indicators

Two datasets were used in this study, the IQ-OTH/NCCD lung cancer dataset and the Kaggle Chest CT image dataset.

The IQ-OTH/NCCD dataset contains CT scans of lung cancer patients at different stages as well as healthy individuals. There are 1197 CT images for 110 instances. Fifty-five of the cases were categorized as normal, forty as malignant, and fifteen as benign (Alyasriy, 2020).

Kaggle Chest CT**:** Lung cancer CT scans can be found in the Kaggle Chest CT dataset. The dataset is organized into three folders: Training, test, and validation. There are four types of CT scans: Normal, squamous cell carcinoma, adenocarcinoma, and big cell carcinoma. There are 1000 CT scans of the chest that show lung cancer. These pictures are a publicly accessible dataset that has been annotated by qualified radiologists. There are 1000 cases, with normal being 215 CT scans, Squamous Cell Carcinoma is 260, Large Cell Carcinoma is 187, and Adenocarcinoma is 338 (Hany, 2024).

Evaluation Metrics

For a thorough quantitative study, the segmentation model's performance was assessed using Accuracy, Precision, Recall, and Specificity. In order to verify the efficacy of our suggested approach, thorough comparisons are made with both traditional and cutting-edge techniques. These methods include UNet, AttUNet, VNet, SwinUNETR, U2-Net, APAUNet, MGNet, and UNet++.

Performance of Proposed Methods

To validate the effectiveness of our proposed method, comprehensive comparisons are performed with both classical and state-of-the-art methods. This paper compares the performance of our proposed model, AWDCE-Net, to other leading lung cancer classification methods. In terms of feature extraction and segmentation accuracy, the precision, recall, F1-score, and accuracy metrics of each model demonstrate their differences. CNN-based models, such as SegNet, ResUNet, UNet, and UNet++, have demonstrated consistent performance in medical picture segmentation and are widely used in real-world applications. Table 1 displays the experimental results of the IQ-OTH/NCCD data set; Tables 2 display the Kaggle Chest CT data set, respectively.

The confusion matrix of multi-class lung cancer CT images of the IQ-OTH/NCCD dataset results of our proposed method is given in Fig. 6, and the KAGGLE CHEST CT data set is given in Fig. 7. The proposed method outperforms other models in its ability to capture details and global features, which helps segment lung nodules more accurately. One may also observe that some methods exhibit high recall but low precision, indicating that these models tend to over-segment and generate excessive false positives. This characteristic behavior is commonly observed, particularly in images with imbalanced foreground-to-background ratios and high similarity between target structures and their adjacent tissues. Our approach overcomes these limitations by integrating multi-scale feature refinement with a multilevel attention mechanism, enabling superior boundary awareness and enhanced contextual understanding.

Table 1: Experimental results of AWDCE-Net and Other models on the IQ-OTH/NCCD Dataset

Models	Accuracy (%)	Precision (%)	Recall (%)	F1-measure (%)
U-Net	86.40	82.52	86.32	83.20
Att-U-Net	98.11	97.67	97.89	97.78
V-Net	97.85	98.81	97.60	97.45
SwinUNETR	97.98	96.67	97.67	97.23
U2-Net	98.05	97.81	98.22	97.81
APAUNet	96.35	96.03	97.13	96.11
MGNet	98.40	98.0	98.56	98.1
UNet++	98.89	98.67	98.78	98.78
Proposed Method **(**AWDCE-Net	99.12	99.18	99.14	99.19

Table 2: Experimental results of AWDCE-Net and Other models on the KAGGLE CHEST CT dataset

Models	Accuracy (%)	Precision (%)	Recall (%)	F1-measure (%)
U-Net	87.63	82.11	86.34	83.34
Att-U-Net	88.11	87.67	87.67	87.78
V-Net	87.85	88.81	86.81	87.45
SwinUNETR	87.98	86.67	88.91	87.23
U^2-Net	88.05	87.81	88.25	87.56
APAUNet	91.35	91.03	91.81	91.11
MGNet	88.40	88.0	88.11	88.19
UNet++	88.89	88.67	88.97	88.78
Proposed Method**(**AWDCE-Net	98.11	98.98	98.67	98.12

Ablation Experiment

In AWDCE-Net, some functional modules were created and utilized in the network to enhance segmentation in order to make up for the performance loss brought on by the decrease in trainable parameters as a result of network light weighting. In this work, the AD module modulates the weight of each pixel by learning local and global relationships between the primary phase (venous phase) and the supplementary phases (non-contrast and arterial phases). The Res block is used to establish global cross-modality associations. This transformer adaptively extracts refined tokens, facilitating more effective feature representation, and the Fuzzy skip connection utilizes fuzzy processing to formulate high-level semantic features and suppress redundant background information, thereby obtaining high-precision lung nodules segmentation results. Figure 8 displays the outcomes of the experiment. After the functional modules are removed, Baseline serves as the network framework's backbone model. Figure 8 shows that the introduction of upgraded convolutional blocks led to varied degrees of overall performance improvement on all three datasets when compared to the backbone network Baseline. Qualitative segmentation results for all comparison approaches are shown in Figure 8. Visual examination shows that for all three datasets, our suggested approach reliably generates segmentation masks that nearly match the ground truth annotations. Our solution outperforms current approaches in border delineation in the Lung dataset, especially when dealing with intricate morphological structures with variable shapes. The majority of approaches, on the other hand, have a tendency to provide fragmented forecasts and deal with the over- or under-segmentation problem.

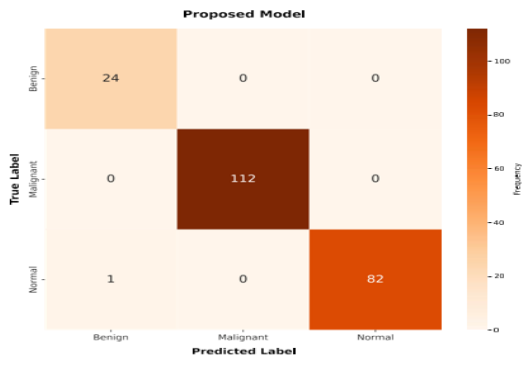

Fig. 6: Confusion matrix for IQ-OTH/NCCD dataset

DOI: 10.3844/jcssp.2026.162.170

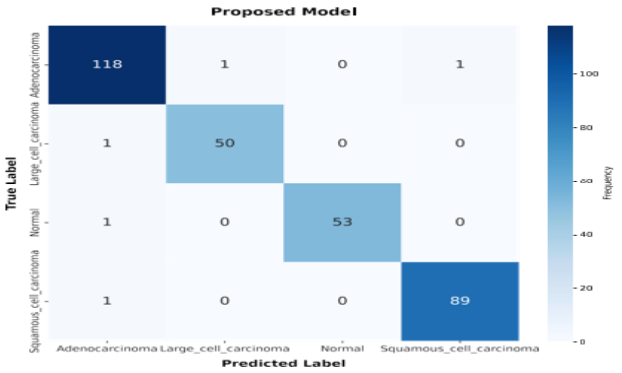

Fig. 7: Confusion matrix for the Chest CT dataset

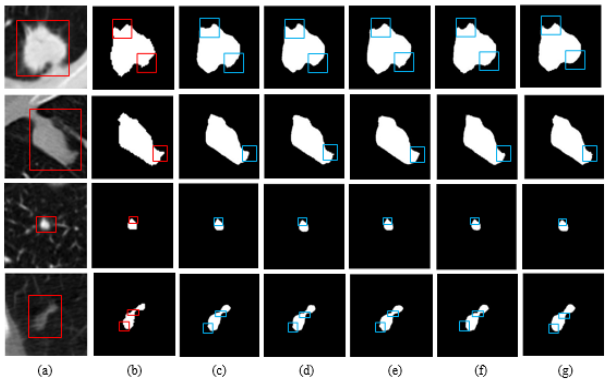

Fig. 8: Visual comparison of ablation experiments. (a) The original CT image of the lung nodule, (b) ground truth, (c) AWDCE-Net, (d) Baseline, (e) Baseline + R1, (f) Baseline + R2, (g) Baseline + (R1+R2)

Grad-Cam Analysis

A key interpretability tool in deep learning is gradient-weighted class activation mapping, or Grad-CAM, which makes it possible to visualize the areas of an input image that most strongly influence the model's predictions. Grad-CAM generates heatmaps that clearly illustrate the model's focal regions by calculating the gradients of a target class in relation to the final convolutional layer. This approach guarantees that the model's decision-making process is in line with clinically significant aspects, promoting transparency and reliability, which makes it especially useful for medical imaging applications like lung cancer diagnosis. Grad-CAM heatmaps for three representative CT scan scenarios benign, malignant, and normal are shown in Figure 9.

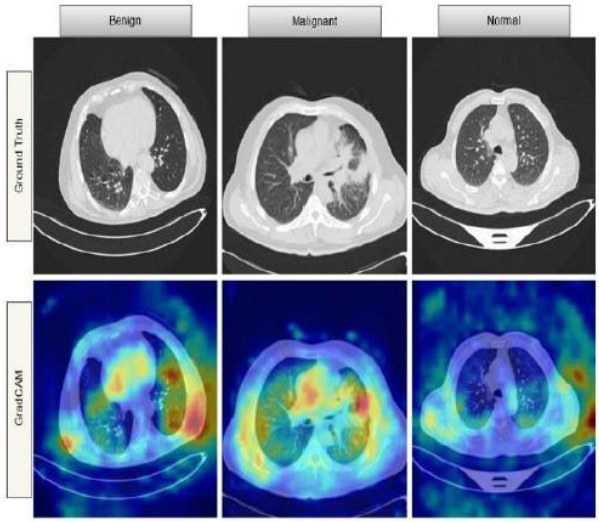

Fig. 9: Grad-Cam Heat Maps for Lung Cancer CT Images

Conclusion

In this paper, we introduced a novel framework for CT image analysis that combines attention-aware aggregation modules with hierarchical feature fusion. Our method's better capacity to capture discriminative characteristics was demonstrated through extensive testing on three public ling datasets, consistently outperforming state-of-the-art techniques in both quantitative and qualitative evaluations. The ablation trials demonstrate how well the suggested modules work to improve segmentation performance and feature representation. These results demonstrate the potential of our methodology for quantitative lesion analysis in ultrasound imaging and clinical diagnosis. A feature refinement module with dense connections was created to mitigate the effects of image noise. It was then applied to additional skip connection paths to maximize feature details and enhance model segmentation performance overall. AWDCE-Net has a high reference value and performs well on a variety of datasets when compared to other top network models in the same field. Although the model has achieved good performance, due to the low overall parameter count of the model, there may be certain limitations in segmentation ability. This approach has the potential to improve early diagnosis of lung cancer, which is important for improving patient outcomes and survival rates. Scalability and viability for practical clinical applications are guaranteed by its lightweight design. To optimize its clinical impact, future work will concentrate on improving the model, expanding its application to different imaging modalities, and evaluating its generalizability across other demographics and datasets.

Acknowledgment

Thank you to the publisher for their support in the publication of this research article. We are grateful for the resources and platform provided by the publisher, which have enabled us to share our findings with a wider audience. We appreciate the efforts of the editorial team in reviewing and editing our work, and we are thankful for the opportunity to contribute to the field of research through this publication.

Funding Information

The authors have not received any financial support or funding to report.

Author's Contributions

Both the authors have equally contributed to this manuscript.

Ethics

This article is original and contains unpublished material. The corresponding author confirms that all of the other authors have read and approved the manuscript and no ethical issues involved.

Reference

Adams, S. J., Stone, E., Baldwin, D. R., Vliegenthart, R., Lee, P., & Fintelmann, F. J. (2023). Lung cancer screening. *The Lancet*, *401*(10374), 390–408. https://doi.org/10.1016/s0140-6736(22)01694-4

Alyasriy, H. (2020). The IQ-OTHNCCD lung cancer dataset. *Mendeley Data*. https://doi.org/10.17632/BHMDR45BH2.1

Bade, B. C., & Dela Cruz, C. S. (2020). Lung Cancer 2020: Epidemiology, Etiology. *Clinics in Chest Medicine*, *41*(1), 1–24. https://doi.org/10.1016/j.ccm.2019.10.001

Bray, F., Laversanne, M., Sung, H., Ferlay, J., Siegel, R. L., Soerjomataram, I., & Jemal, A. (2024). Global cancer statistics 2022: GLOBOCAN estimates of incidence and mortality worldwide for 36 cancers in 185 countries. *CA: A Cancer Journal for Clinicians*, *74*(3), 229–263. https://doi.org/10.3322/caac.21834

Cheng, J.-Z., Ni, D., Chou, Y.-H., Qin, J., Tiu, C.-M., Chang, Y.-C., Huang, C.-S., Shen, D., & Chen, C.-M. (2016). Computer-Aided Diagnosis with Deep Learning Architecture: Applications to Breast Lesions in US Images and Pulmonary Nodules in CT Scans. *Scientific Reports*, *6*(1), 24454. https://doi.org/10.1038/srep24454

Ciello, A. del, Franchi, P., Contegiacomo, A., Cicchetti, G., Bonomo, L., & Larici, A. R. (2017). Missed lung cancer: when, where, and why? *Diagnostic and Interventional Radiology*, *23*(2), 118–126. https://doi.org/10.5152/dir.2016.16187

De Margerie-Mellon, C., & Chassagnon, G. (2023). Artificial intelligence: A critical review of applications for lung nodule and lung cancer. *Diagnostic and Interventional Imaging*, *104*(1), 11–17. https://doi.org/10.1016/j.diii.2022.11.007

Gould, M. K., Donington, J., Lynch, W. R., Mazzone, P. J., Midthun, D. E., Naidich, D. P., & Wiener, R. S. (2013). Evaluation of Individuals With Pulmonary Nodules: When Is It Lung Cancer? *Chest*, *143*(5), e93S-e120S. https://doi.org/10.1378/chest.12-2351

Hanna, T. N., Lamoureux, C., Krupinski, E. A., Weber, S., & Johnson, J.-O. (2018). Effect of Shift, Schedule, and Volume on Interpretive Accuracy: A Retrospective Analysis of 2.9 Million Radiologic Examinations. *Radiology*, *287*(1), 205–212. https://doi.org/10.1148/radiol.2017170555

Hany, M. (2024). Chest CT-Scan Images Dataset. *Kaggle Datasets*. https://www.kaggle.com/datasets/mohamedhanyyy/chestctscan-images

Jha, D., Smedsrud, P. H., Riegler, M. A., Johansen, D., Lange, T. D., Halvorsen, P., & D. Johansen, H. (2019). ResU-Net++: An Advanced Architecture for Medical Image Segmentation. *Proceedings of the IEEE International Symposium on Multimedia*, 225–255. https://doi.org/10.1109/ism46123.2019.00049

Long, J., Shelhamer, E., & Darrell, T. (2015). Fully Convolutional Networks for Semantic Segmentation. *2015 IEEE Conference on Computer Vision and Pattern Recognition (CVPR)*, 3431–3440. https://doi.org/10.1109/cvpr.2015.7298965

Lundervold, A. S., & Lundervold, A. (2019). An overview of deep learning in medical imaging focusing on MRI. *Zeitschrift Für Medizinische Physik*, *29*(2), 102–127. https://doi.org/10.1016/j.zemedi.2018.11.002

McDonald, R. J., Schwartz, K. M., Eckel, L. J., Diehn, F. E., Hunt, C. H., Bartholmai, B. J., Erickson, B. J., & Kallmes, D. F. (2015). The Effects of Changes in Utilization and Technological Advancements of Cross-Sectional Imaging on Radiologist Workload. *Academic Radiology*, *22*(9), 1191–1198. https://doi.org/10.1016/j.acra.2015.05.007

Nitha, V. R., & Vinod Chandra, S. S. (2024). Novel CEFNet framework for lung disease detection and infection region identification. *Biomedical Signal Processing and Control*, *96*, 106624. https://doi.org/10.1016/j.bspc.2024.106624

Ronneberger, O., Fischer, P., & Brox, T. (2015). U-net: Convolutional networks for biomedical image segmentation. *Medical Image Computing and Computer-Assisted Intervention – MICCAI 2015*, 234–241.

Siegel, R. L., Miller, K. D., Fuchs, H. E., & Jemal, A. (2022). Cancer statistics, 2022. *CA: A Cancer Journal for Clinicians*, *72*(1), 7–33. https://doi.org/10.3322/caac.21708

Sluimer, I., Schilham, A., Prokop, M., & van Ginneken, B. van. (2006). Computer analysis of computed tomography scans of the lung: a survey. *IEEE Transactions on Medical Imaging*, *25*(4), 385–405. https://doi.org/10.1109/tmi.2005.862753

Tharwat, M., Sakr, N. A., El-Sappagh, S., Soliman, H., Kwak, K.-S., & Elmogy, M. (2022). Colon Cancer Diagnosis Based on Machine Learning and Deep Learning: Modalities and Analysis Techniques. *Sensors*, *22*(23), 9250. https://doi.org/10.3390/s22239250

Zhou, Z., Siddiquee, M. M. R., Tajbakhsh, N., & Liang, J. (2020). UNet++: Redesigning Skip Connections to Exploit Multiscale Features in Image Segmentation. *IEEE Transactions on Medical Imaging*, *39*(6), 1856–1867. https://doi.org/10.1109/tmi.2019.2959609